Report 1997:2

Effects of Anthropogenic Emissions on Tropospheric Ozone and its Radiative Forcing

T. Berntsen, I.S.A. Isaksen, J.S. Fuglestvedt, G. Myhre, T. Alsvik Larsen, F. Stordal, R.S. Freckleton and K.P. Shine

Effects of Anthropogenic Emissions on Tropospheric Ozone and its Radiative Forcing

T. Berntsen[1,2], I.S.A. Isaksen[1,2], J.S. Fuglestvedt[2],
G. Myhre[1], T. Alsvik Larsen[1], F. Stordal[3,1],
R.S. Freckleton[4] and K.P. Shine[4]

February 1997

[1] Department of Geophysics, University of Oslo, Norway
[2] CICERO - Center for International Climate and Environmental Research - Oslo, Norway
[3] Norwegian Institute for Air Research (NILU)
[4] University of Reading, UK

Abstract

Tropospheric ozone changes since pre-industrial times due to changes in emissions have been calculated by the University of Oslo global 3-D photochemical model. The radiative forcing caused by the increase in ozone has been calculated by two independent radiative transfer models; the University of Reading model (Reading), and the University of Oslo/NILU model (OsloRad). Significant increases in upper tropospheric ozone concentrations are found at northern mid-latitudes (15-40 ppbv, depending on season) at about 10 km altitude. In the tropical regions, the largest increase (about 20 ppbv for all seasons) is found at about 15 km altitude. The increase is found to be caused mainly by enhanced in-situ production due to transport of precursors from the boundary layer, with a smaller contribution from increased transport of ozone produced in the boundary layer. The lifetime of ozone in the troposphere decreased by about 35 % due to enhanced concentrations of HO_2. The calculated increase in surface ozone in Europe is found to be in good agreement with observations. The calculations of radiative forcing include the effect of clouds and allow for thermal adjustment in the stratosphere. The global and annual averaged radiative forcing at the tropopause from both models (0.28 W/m^2 and 0.26 W/m^2, for the OsloRad and Reading models respectively) are in the lower part of the estimated range given in IPCC (1995). The calculated radiative forcing is similar in magnitude to the negative radiative forcing by sulphate aerosols, but displaced southward in source regions at northern mid-latitudes. The increase in tropospheric ozone is calculated to have cooled the lower stratosphere by up to 0.9 K, with possibly half of this cooling occuring in the past two to three decades.

Table of Contents

1. Introduction

Since the onset of the industrial revolution the emissions of man-made pollutants have increased substantially. This is believed to have caused a significant radiative forcing of climate, mainly through the influence of increases in the long lived greenhouse gases carbon dioxide, methane, nitrous oxide and the chlorofluorocarbons (CFCs). However, there have also been increases in the emissions and concentrations of chemically more active gases which react to give ozone in the troposphere, namely NO_x ($NO+NO_2$), CO and the hydrocarbons. Enhanced concentrations of tropospheric ozone have been found both through observations and model calculations (e.g. Volz and Kley,1988; Anfossi et al., 1991; Logan, 1985; Oltmans and Levy, 1994; Marenco et al., 1994). Model calculations (Hauglustaine et al., 1994; Lelieveld and van Dorland, 1995; Müller and Brasseur, 1995; Forster et al., 1997) show that there are close connections between the increase in the emissions and the increase in ozone. To assess the radiative forcing following this increase, knowledge of the global distribution of ozone changes is necessary. Due to the very limited observations of ozone during the pre-industrial period, and limited coverage of upper tropospheric ozone particularly in the tropics at present, simulations by three-dimensional (3D) chemical tracer models (CTMs) are now being used to calculate the ozone distribution.

The potential climatic effect of the ozone change is reported here using the concept of *radiative forcing*, which essentially indicates the change in the energy available to the surface-troposphere system. As discussed in, for example, IPCC (1994; 1995), Cox et al. (1995) and Hansen et al. (1997), radiative forcing gives a useful first order estimate of the potential significance of climatic change mechanisms; it allows for the comparison of different mechanisms, and also, importantly, for different evaluations of their effect to be readily intercompared. However, there are clear limitations. The geographical distribution of forcing is not tightly related to the geographical distribution of the climate response and care must be taken in comparing the forcings from different mechanisms which may differ in size and geographical distribution. For instance, the forcing from the well-mixed gases may initiate climate responses that differ significantly from the responses to the more heterogeneous (vertically and horizontally) forcing caused by tropospheric ozone or sulphate aerosols.

As pointed out by Wang and Sze (1980) and Lacis et al. (1990) the radiative forcing is most sensitive to changes in ozone concentrations in the vicinity of the tropopause. In addition, changes in the tropical regions are of particular interest due to the high temperature difference between the surface and the tropopause, the generally lower cloudiness than in mid-latitude regions and the large area covered. All these factors contribute to make the tropics a region of particular importance for the globally averaged radiative forcing caused by changes in tropospheric ozone.

Based on observations and model studies, IPCC (1994) gives a range of 0.2 - 0.6 W/m^2 for the radiative forcing due to changes in tropospheric ozone since pre-industrial times (IPCC,1994, and references therein). In some of the previous studies the impact of clouds has been neglected, which will, as we discuss later, tend to overestimate the impact of increased tropospheric ozone on the radiative forcing. In the results presented here, cloud information from ISCCP has been used to account for the effect of clouds.

In this study the University of Oslo global 3-D CTM has been used to calculate changes in chemical composition of the troposphere due to changes in emissions since 1850. The intention has been to study the impact of increased emissions of NOx, CO and CH_4, on the radiative forcing of climate, by introducing the ozone perturbation calculated by the CTM in

two different radiative transfer models. Other factors that could influence tropospheric ozone, and which might have undergone changes since pre-industrial times, include changes in photolysis rates due to a decrease in total ozone (Fuglestvedt et al., 1994; Bekki et al., 1994), changes in water vapour and temperature due to climatic changes (Fuglestvedt et al., 1995; Wang et al., 1996), changes in land-use that could have affected deposition velocities, trends in tropopause fold events (Haugland, 1995), etc. These have not been considered in this work.

The CTM has previously been applied to study the impact of increasing emissions of NOx and non-methane hydrocarbons (NMHCs) in south east Asia on ozone and radiative forcing (Berntsen et al., 1996). In the present study, the CTM has been run with emissions according to 1850 and 1990 conditions respectively. In the Reading model climatological ozone fields based on observations were used in the 1990 case, and the 1850 case was constructed by subtracting the delta ozone fields calculated by the CTM from the 1990 climatology. In the OsloRad model, the 1850 and 1990 ozone fields obtained from the CTM were used directly.

2. Model description

2.1 The chemical tracer model

The CTM has a resolution of 8 by 10 degrees (latitude vs. longitude) and 9 vertical layers below 10 hPa. The vertical resolution in the vicinity of the tropopause is about 3 km at mid and high latitudes, and about 4.5 km in the tropics. The transport formulation is similar to Prather et al. (1987). It includes three-dimensional advection, calculated by the 'second order moments' method of Prather (1986), as well as rapid vertical mixing by convective transport. This is very important, as it allows short-lived species (e.g. NO_x and NMHCs) emitted from the surface to be deposited in the upper troposphere. The strength of the deep convective transport is quite uncertain. Jacobs et al. (1997) have compared vertical mixing of ^{222}Rn in various CTMs, including the GISS/H/I model which has a very similar transport parameterization as our CTM, concluding that the simulated deep convection in the troposphere is within the constraints offered by seasonal averages of ^{222}Rn concentrations at different altitudes. However, the GISS/H/I model was found to be among the more efficient models in bringing ^{222}Rn from the surface to the upper troposphere.

A comprehensive photochemical scheme with about 50 chemical components and 110 gas-phase reactions has been incorporated to simulate the photochemistry of the troposphere. Within the troposphere, the chemistry with a full diurnal cycle is calculated with a quasi steady-state approximation method (QSSA), with iterations for the short-lived species (Hesstvedt et al., 1978). In the stratosphere, concentrations of ozone, NO_x and HNO_3 are fixed according to the observed distribution of these species. The circulation within the whole model domain up to 10hPa then generates an internally consistent cross-tropopause flux. Photolysis rates are calculated using the two-stream approximation method described in Isaksen et al. (1977), with updates to incorporate scattering by cloud droplets and aerosols according to Jonson (1993). The model uses pre-calculated meteorological input data with 8-hour time resolution from a one year climate simulation with the NASA/GISS GCM. This means that synoptic scale variability is resolved, in contrast to other 3-D CTMs used in previous studies of changes since pre-industrial times (i.e. the MOGUNTIA model (Lelieveld and van Dorland, 1995) and the IMAGES model (Müller and Brasseur, 1995)). The continuity equation is solved by an operator splitting procedure with a one hour timestep for the transport, and 30 minutes for the chemistry. A thorough discussion of the model is given in Berntsen and Isaksen (1997).

One major change has been made to the CTM for this study. In Berntsen et al.(1996) and Berntsen and Isaksen (1997) the CTM was run with a fixed tropopause height taken to be at the boundary between model layers 7 and 8 ($\approx$13.7 km altitude) for all latitudes. Longitudinally homogeneous ozone concentrations were set in the layers above according to observed ozone concentrations. As pointed out in the introduction, changes in the upper troposphere in the tropics are potentially very important for climate. Therefore, as the tropopause height is considerably higher in the tropics, we have increased the tropopause height equatorward of 32° to coincide with the boundary between model layer 8 and 9 ($\approx$18.5 km altitude) in the version of the CTM applied in this study.

2.2 Radiative transfer models

Radiative forcing calculations were performed with two different models, denoted Reading and OsloRad, using the calculated ozone changes described in Section 4. The radiation schemes used in the OsloRad and by Reading models were independently produced, as were the baseline climatologies of temperature, humidity and cloud amount. Thus comparison of the

results from the two models provides a useful cross-check and, as will be seen, the differences in the results are important in indicating the parameters to which the ozone radiative forcing is sensitive.

The Reading radiation schemes are a 10 cm^{-1} standard narrow band model in the thermal infrared (Shine, 1991) using all the lines of water vapour, carbon dioxide, ozone, nitrous oxide and methane between 0 and 3000 cm^{-1} in the HITRAN-92 spectral line data (Rothman et al., 1992) and a 4-stream discrete-ordinate model (Stamnes et al., 1988) at solar wavelengths, with a 5 nm resolution in the ultraviolet and a 10 nm resolution in the visible (Forster and Shine, 1997). Clouds can be included in all wavelength regions. These radiation schemes have previously been used to calculate the radiative forcing due to changes in tropospheric ozone by Forster et al. (1997).

The OsloRad thermal infrared radiation scheme is a broad band model (Stordal, 1988, Myhre and Stordal, 1997). The model includes about 50 bands among all the trace gases of importance for modelling of the terrestrial infrared radiation. For ozone the main band at 9.6 µm and the spectroscopically weaker band at 14 µm are included. At ultraviolet and visible wavelengths a model using the discrete ordinate method (Stamnes et al. 1988) is used. In these calculations 8-streams and a spectral resolution of 15 nm in the range 176-850 nm is used. Clouds are included in both the thermal infrared scheme and the shortwave scheme.

The Reading and OsloRad models have been compared for an identical tropospheric ozone change and identical temperature and water vapour profiles. The ozone change used in both models was taken from the model comparison of radiative forcing due to changes in ozone in Shine et al. (1995) where the Reading results are also given, while results from the OsloRad model are given in Stordal et al. (1996). The thermal infrared radiative forcings were almost equal (0.104 Wm^{-2}/0.105 Wm^{-2}) and within 6% of the line-by-line results reported in the comparison. In the shortwave the updated Reading code (see Section 4 of Shine et al. 1995) gives identical results (0.023 Wm^{-2}) to OsloRad.

The Reading calculations in this work are performed using monthly-mean fields on a 10° latitude by 20° longitude grid with a vertical resolution of 17 to 19 layers (depending on surface pressure); the top level is at 1 hPa. The tropopause was specified at each point as the level at which the lapse rate is 2 K km^{-1}. Forcings were calculated for January, April, July and October; the annual average reported here is the average of these four months.

The OsloRad calculations are performed with a horizontal resolution of 2.5° in longitudinal and latitudinal direction and a vertical resolution of 25 layers. The tropopause level was specified where the temperature gradient changes sign, except at high latitudes where a weak negative gradient is allowed even above the tropopause (typically 8-10 km). The calculations are performed with monthly mean data and for each of the 12 months. The annual average in the OsloRad model is an average of the 12 months.

3. Experimental setup

Two 17 month model runs starting on 1. April with emissions according to 1850 and 1990 conditions respectively have been done. The data for the last 12 months has been used in the analysis. For all components except methane, five month spin-up is sufficient to reduce the difference between calculated concentrations in month 5 and 17 of the experiment to less than 3%. The methane concentrations were initialized in each experiment according to observations. For the pre-industrial period, the methane concentration was set to 820 ppbv, while for present day conditions the methane concentration was set to 1700 ppbv (IPCC, 1994). Due to the short integration period compared with the lifetime of methane, the calculated methane concentrations are mainly influenced by the initial concentrations, thus they are not discussed further.

3.1 Chemistry and emissions

The photochemical production of ozone in the troposphere is significantly larger than the flux from the stratosphere (Feshenfeldt and Liu, 1993; Berntsen and Isaksen, 1997). The ozone production in the troposphere is caused by oxidation of NO to NO_2 by HO_2 or RO_2 radicals and the subsequent photolysis of NO_2 through the reactions:

$NO + HO_2/RO_2 \rightarrow NO_2 + OH/RO$	*R1*
$NO_2 + h\nu \rightarrow NO + O$	*R2*
$O + O_2 + M \rightarrow O_3 + M$	*R3*
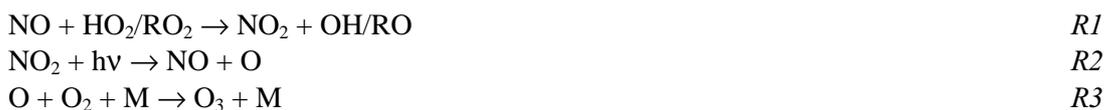
The ozone production in the free troposphere is generally limited by the abundance of NOx. Methane and CO are the main sources of the HO_2 and RO_2 radicals necessary to oxidise NO to NO_2 and cause ozone production. Realistic emission inventories of NOx and CO are therefore important in simulating ozone changes in the free-troposphere. The emission inventories of CO, NOx and methane for both the 1850 and 1990 case in this study are based on the emission rates used by Lelieveld and van Dorland (1995). A major source of CO in their inventory is through NMHC oxidation. As our chemical scheme includes NMHC chemistry, the CO emissions have been reduced and emissions of NMHCs are included accordingly. Table 1 shows the global and annual mean emissions used in this study.

Table 1. Emission rates applied in the model study. *Sensitivity experiment with no anthropogenic NMHC emissions. **Includes emissions from vegetation, soils, wildfires and ocean.

Species	1850	1990
NO_x (Tg(N)/yr) Surface	11.6	37.8
Lightning	5.2	5.2
Aircraft	0.0	0.6
CO (Tg/yr) Total	290	1400
Anthropogenic	0	810
Biomass burning	100	400
Natural sources**	190	190
Isoprene (Tg/yr)	267	205
Other NMHC[$] (Tg/yr)	175.7 (64.8*)	175.7

[$]Other NMHCs includes ethane, butane, hexane, etene, propene and m-xylene.

The estimate of NO_x emissions from aircraft is taken from British Aerospace (C. Hume, private communication). The estimate is about 30% higher than the NASA estimate applied by Brasseur et al. (1996). Due to increased population and increased farming, it has been hypothesized in this study that isoprene emissions were 30% higher in 1850 due to the reduction in the areas covered by deciduous forests between 1850 and 1990. Emissions of NMHCs are very uncertain, in particular the emissions from natural sources. In both the 1850 and 1990 cases, the emissions of NMHCs other than isoprene were kept constant, as it was expected that free-tropospheric ozone was less sensitive to these emissions than those of NOx, CO and CH_4. To estimate the potential impact of this assumption, the 1850 case was re-run with all anthropogenic NMHC emissions assumed to be zero (giving a total for other NMHC-emissions of 64.8 Tg/yr, not including isoprene). The effect on the calculated changes of ozone was less than ±3% in the free troposphere, and the corresponding changes in the annual and global mean instantaneous thermal infrared radiative forcing less than 0.01 W/m^2 (about 3%).

4. Chemical composition of the troposphere

4.1 Pre-industrial concentrations

In the 1850 case the maxima in the surface CO concentrations (Figure 1) are found over tropical continental regions due to relatively high emission rates of CO from biomass burning and also high production from oxidation of natural hydrocarbons. There is a decrease towards northern mid-latitudes, where CO concentrations between 25-30 ppbv are found. Maxima in the CO concentrations in the tropics were also found in previous studies by Lelieveld and van Dorland (1995) and Müller and Brasseur (1995). The maxima shown in Figure 1 are similar to what was reported by Müller and Brasseur (40-60 ppbv, versus 50-70 ppbv in this study). The difference is partly explained by the somewhat lower methane concentrations used in their study (650 ppbv versus 820 ppbv in this study). Lelieveld and van Dorland use similar emission inventories, however, their CO concentrations are significantly higher (120 ppbv) than in this study. This is probably caused by a combination of more efficient vertical transport by deep convective clouds, higher OH concentrations (see section 4.3) and chemical production of CO from oxidation of NMHCs at higher elevations in this model. During NH winter (not shown) the CO distribution becomes more evenly distributed between the tropics and the NH mid-latitudes due to increased lifetime at higher latitudes during winter. In the upper troposphere, there are also maxima over the continents in the tropics (50 ppbv at about 12 km altitude in June), a minimum over the tropical Pacific (25 ppbv), and decreasing CO concentrations towards the poles (25 ppbv at 60°N in June).

The surface NOx concentrations in the 1850 case (Figure 2) are quite homogeneous in the boundary layer over continental regions, ranging from about 100 pptv at mid-latitudes and 200-300 pptv in the continental boundary layer in the tropics. In the marine boundary layer and in subtropical dessert regions, large regions with NOx concentrations below 5 pptv are found. Active convection in the tropics, in particular over continental regions, gives a NOx maximum in the upper troposphere over Africa and South America. Rapid vertical transport of NOx-rich surface air and high lightning activity in convective cells, contribute to the enhanced upper tropospheric NOx concentrations. Downward transport of NOx-rich air from the stratosphere and more rapid photolysis of HNO_3 at higher altitudes contribute to an upper tropospheric NOx-maximum in all regions.

Figures 3 and 4 show the calculated monthly mean concentration of ozone close to the surface and in the upper troposphere for June in the 1850-case. Maxima in the surface concentrations of about 15 ppbv, are found on the west coast of the continents in the tropics due to in situ production over the continents and the easterly flow in the trade winds. There is a third maximum over northern India and the Himalayas, due to a combination of downward mixing of stratospheric air, probably caused by the influence of the mountain range on the dynamic processes in the GCM, and in situ production.

In the upper troposphere, ozone concentrations are generally low (5-30 ppbv) in the tropics, in particular over the Pacific. The *net chemical ozone production* (production minus chemical loss, deposition not included) is positive in the upper troposphere in the tropics and sub-tropics, 0-0.5 ppbv/day over marine background regions and 2-6 ppbv/day over continental regions, where the NOx levels are enhanced due to extensive convection. At higher latitudes the net ozone production becomes negative. Nevertheless, ozone concentrations increase towards the poles in both hemispheres due to stratosphere/troposphere exchange. The concentrations are generally about 30% higher in the northern hemisphere, due to more extensive downward mixing of stratospheric air (Roelofs and Lelieveldt, 1997).

4.2 Changes since pre-industrial times

4.2.1 Ozone precursors

Concentrations of species emitted due to human activity (CO, NOx) show large increases in the 1990 case. Figure 5 shows the calculated changes in zonally averaged concentrations of CO in June. The increases are largest in the boundary layer in the source regions at northern mid-latitudes. In the southern hemisphere the increase is largest in the upper troposphere. Hence, the large increases in emissions at northern mid-latitudes, which are transported to the southern hemisphere in the upper part of the ITCZ, are an important reason for the CO increases in the southern hemisphere together with the increased source of CO through methane oxidation. The calculated CO concentrations in the 1990 case have been compared with observations (Novelli et al., 1992). At northern mid-latitudes, observations indicate CO levels of 100-120 ppbv in June at background locations, while the model predicts about 110 ppbv for the zonal average mixing ratio of CO in June. In the tropical Pacific (Samoa) about 60 ppbv of CO is observed in June, while the CTM gives about 55 ppbv.

The largest increases in CO concentrations (150 ppbv in the zonal average) are found during the northern hemisphere winter (at mid-latitude source regions and extending to high latitudes) due to slower vertical mixing and the long chemical lifetime caused by the low OH concentrations. The CO levels in the 1990 case at northern hemisphere background locations during winter (175-200 ppbv) are somewhat lower (30-50 ppbv) than indicated by observations (Novelli et al, 1992), which is probably due to an underestimation of the anthropogenic sources of CO.

The strongest increase of NOx in the boundary layer (Figure 6) is mainly confined to the industrial regions in the northern hemisphere. At higher latitudes the lifetime of NOx is longer, due to the rapid decrease in OH concentrations with latitude, and the ventilation of the boundary layer is slower. These effects cause a poleward shift in the maximum concentration change compared with the maximum change in emissions. The regional increase of NOx in the upper troposphere (Figure 7) over north America and south east Asia is caused by active deep convection to this altitudes in the CTM (model layer 7, approximate altitude 10.3-13.7 km). Over Europe the convection, in the CTM, does not extend to the same altitudes, but rather to the layer below. In the tropics, the convection extends even higher (to model layer 8, approx. 13.7-18.5 km altitude). Maximum increases of NOx in the free troposphere correspond with the maximum altitudes of the convective activity in each region. NOx emissions from aircraft in the 1990 case make a significant contribution to the enhanced NOx concentrations in the upper troposphere, in particular in the north-Atlantic flight corridor with a plume extending eastward over Russia. In a separate model experiment, with no aircraft emissions in a simulation of present atmospheric conditions, negligible influence on NOx in the planetary boundary layer (PBL) and 4-40% lower NOx concentrations in the middle troposphere (3-6.5 km) were found (Jaffe et al., 1997).

4.2.2 Net ozone production

The increases in CH_4, CO and NOx concentrations since pre-industrial times, lead to increased ozone production in the CTM. The changes in net chemical ozone production (PO_3; difference between production and loss, deposition not included) are shown in Figures 8 and 9. There is generally an increase in the production throughout the troposphere in the CTM. However, as the loss increases with increasing ozone concentrations, the enhanced ozone concentrations in the 1990 case and transport of ozone to regions with weak production give rise to negative changes in the net chemical production in some regions.

The ozone production is a strongly non-linear function of precursor concentrations, in particular of the NOx concentration (e.g. Isaksen et al., 1978; Lin et al., 1988) and the amount

of solar radiation. Due to the large spatial variation in the source strength, the efficiency of transport mechanisms and background NOx concentrations, there are large spatial and temporal variations in the change in ozone production. There is a distinct spatial correlation between changes in NOx concentrations and the corresponding changes in net ozone production (Figures 6-9) both in the boundary layer and in the upper troposphere.

In June, the maximum increase in net chemical ozone production in the boundary layer is found over industrial regions at northern mid-latitudes, especially over the southern United States and east Asia, and over tropical regions of Africa and South-America due to increased emissions from biomass burning (Figure 8). The maxima at northern mid-latitudes are shifted southward compared with the NOx maxima, due to the positive correlation between solar insolation and ozone production in polluted airmasses, higher emissions of natural hydrocarbons at lower latitudes (mainly isoprene) and the higher ozone production efficiency per NOx molecule oxidised at low NOx concentrations. In the boundary layer over north-western Europe there was a net chemical ozone production of about 2 ppbv/day in the 1850 case. In this region there is a decrease in net ozone production in the 1990 case, giving a small net chemical loss of ozone. This is due to high emission rates of NO, lower solar insolation at these latitudes and increased ozone concentrations (15-20 ppbv, see Figure 11). The two first factors enhance the effect of titration of ozone through,

$$O_3 + NO \rightarrow O_2 + NO_2 \hspace{4cm} R4$$

as the amount of peroxyradicals (HO_2, RO_2) which through reaction $R1$ lead to ozone production, are limited by the amount of OH and thereby on solar radiation through the production of OH.

$$O_3 + h\nu \rightarrow O(^1D) + O_2 \hspace{1cm} \lambda < 320 \text{ nm} \hspace{3cm} R5$$
$$O(^1D) + H_2O \rightarrow 2 \text{ OH} \hspace{6cm} R6$$

In the 'clean' marine boundary layer, NOx concentrations are often lower than the threshold value for ozone production ($\approx$5-10 pptv of NO, Crutzen, 1987). The enhanced CO and methane concentrations in the 1990 case are sources of HO_2 radicals, which, at low NOx concentrations, tend to give with a net chemical loss of ozone through;

$$O_3 + HO_2 \rightarrow OH + 2O_2 \hspace{4cm} R7$$

In the upper troposphere, an enhanced net chemical ozone production is calculated at all latitudes north of 60°S in June (Figure 9). The reduction at high southern latitudes is very small, and has negligible influence on the ozone concentrations. The increases in the net production of ozone in the upper troposphere are closely related to the increases in NOx concentrations, with a small equatorward shift as was the case in the boundary layer. The maximum increase is about a factor of 5 lower than in the boundary layer. However, if the increases are normalised to the increase in NOx, the increase is higher in the upper troposphere.

A positive net chemical ozone production in the boundary layer and in the upper troposphere is calculated (table 2). In the middle troposphere (1.4-7.4 km) a net chemical loss of ozone is found due to the low NOx concentrations in this altitude region. The ozone flux across the tropopause, which consists of a large influx from the stratosphere and a much smaller flux from the troposphere at low latitudes, decease slightly in the 1990 case, due to enhanced ozone concentrations in the upper troposphere.

Table 2. Calculated ozone budget in the 1850 and the 1990 case. Net chemical ozone production is devided into the planetary boundary layer (PBL, below approx. 1.4 km), middle troposphere (MT, approx. 1.4-7.4 km) and upper troposphere (UT, approx. 7.4-13.7 km at mid-latitudes, 7.4-18.5 km at low latitudes)

Year	Net ozone production (Tg/yr)			Deposition (Tg/yr)	Across tropopause flux (Tg/yr)
	PBL	MT	UT		
1850	223	-341	254	-503	367
1990	698	-633	692	-1100	343

The calculated increase in the ozone production could be significantly influenced by the background NOx concentrations due to the non-linearities. Jaffe et al. (1997) have compared NOx and NOy concentrations in the model with observations and with other models. There seems to be a tendency for the CTM to underestimate free-tropospheric NOx levels. The reason for this is not quite clear, but could partly be due to problems in the measurement of NOx and NOy from aircrafts (Crawford et al., 1996; Crosley et al.,1996), and partly due to underestimation of the lightning source (Price et al., 1997a and 1997b) Also, recent investigations (Borrmann et al., 1996; Reichardt et al., 1996, Hauglustaine et al., 1996; Lary et al., 1997) indicate that heterogeneous processes on cirrus cloud ice particles and carbonaceous aerosols, which are poorly known and not included in global models, could have significant impact on the chemistry in this region of the atmosphere.

It is not clear how the NOx underestimate will influence the results presented in this paper. If the underestimation is due to errors in the removal rates of NOx during transport from the planetary boundary layer to the upper troposphere being too rapid, this should apply in a similar way to the perturbation of surface sources. The perturbation in the free tropospheric NOx concentrations caused by an increase in surface emissions, will then tend to be too small; however, the non-linear increase of ozone production efficiency with decreasing NOx concentrations would partly counteract this. On the other hand, the relative importance of increases in sources emitting NOx directly at these altitudes (i.e. from aircraft in the 1990 case) is likely to be too strong, since the relative contribution of these sources to the NOx levels could be overestimated.

4.2.3 Ozone in the free troposphere

The free tropospheric ozone in the model has been compared with ozone sonde data given by Komhyr et al. (1992). In the northern hemisphere the CTM tends to underestimate the observed values below 300 hPa by 10-15 ppbv during summer. At higher altitudes and during winter the agreement is quite good. In the southern hemisphere, there is also a tendency in the model to underestimate ozone in the free troposphere by 10-15 ppbv throughout the year (Berntsen and Isaksen, 1997).

The changes in monthly mean mixing ratio of ozone are shown in Figures 10 and 11. Figure 10 shows the changes in zonally averaged values for June and December, while Figure 11 shows changes in the lowest model layer and in model layer 7 (approx. 10.3 to 13.7 km altitude) for June. The largest increases in the zonally averaged mixing ratios are found in the altitude region just below the tropopause at all latitudes, except during southern hemisphere winter when there is a fairly uniform increase throughout the troposphere. In the tropics the calculated increase is about 20 ppbv between about 14 and 18 km altitude, with no marked seasonal cycle. The largest increase in the zonal mean mixing ratio is found at northern mid-latitudes, where the model calculates increases of up to 40 ppbv at 50°N in June. Due to the

strong zonal winds and the extended lifetime of ozone in the mid-latitude upper troposphere, the increase is fairly homogeneous in these regions.

Figure 12 shows the change in the annual mean vertically integrated tropospheric column ozone content in dobson units (DU). The increases are clearly influenced by the increased ozone concentrations in the boundary layer over the industrialised regions in the northern hemisphere. The increases are, however, larger at lower latitudes than indicated by Figure 11a. This is mainly due to the influence of the ozone increase at higher altitudes in the tropics, but also due to the seasonal cycle of the changes in ozone.

The increase in the upper troposphere is caused by two factors :

- Increased vertical flux of ozone produced by photochemical processes in the boundary layer.
- Increased *in-situ* ozone production due to increased concentrations of ozone precursors caused by rapid convective transport from the boundary layer and emissions of ozone precursors from aircraft.

The contribution from each of these processes depends on the correlation between the distribution of deep convection and emissions of ozone precursors, differences in the lifetime of ozone at different altitudes and differences in the background NOx concentrations. To facilitate an evaluation of the cause of upper tropospheric ozone increase, the most relevant budget terms are given in Table 3. The net chemical production increases significantly both in the boundary layer and in the upper troposphere between the 1850 and the 1990 case. The relative increase is strongest in the upper troposphere at mid and high latitudes (32°-90°) in the northern hemisphere due to the close balance between production and loss in the 1850 case (low net ozone production) and the large increase in NOx emissions from aircraft and thereby ozone production in the 1990 case. The least pronounced relative increase is in the low-latitude (LL, 32°S-32°N) regions (the tropics and sub-tropics) of the southern hemisphere during summer (cf. Figure 9 and section 4.2.2).

The CTM calculates a net downward flux of ozone averaged over area and season for each of the four latitude bands given in Table 3, except for the present day northern LL region during summer. Except for the LL region in the northern hemisphere, the CTM gives a general increase in the net downward transport of ozone into the boundary layer since 1850. The mixing of air between the boundary layer and the free troposphere does not change between the 1850 and the 1990 case in this experiment. This means that on the average (seasonally and over the four latitude bands) the increased ozone concentrations in the free-troposphere dominate over the increased concentrations in the boundary layer (cf. Figure 10). The increase in the upward flux of ozone from the northern hemisphere LL region, even if the increase in ozone concentrations becomes larger with altitude (Figure 10a), is caused by a correlation between the regions of upward transport in the equatorial Walker-circulation (over the continents and the western Pacific) and the regions with largest increase in surface ozone (Figure 11a). However, the increase in net upward transport of ozone is much smaller than the increase in net chemical production in the upper troposphere (Summer: 31-(-8.7) =39.7 Tg/yr vs. 189-82=107 Tg/yr). This means that in this CTM, the increased *in-situ* production accounts for the main contribution to the increased ozone concentrations in the upper troposphere at all latitudes.

Table 3. Net chemical production (PO$_3$) of ozone in the planetary boundary layer (model layer 1 and 2, below ≈1.5 km altitude) and in the upper troposphere (UT, model layer 6 and above, above ≈7 km altitude) and net upward flux of ozone from the planetary boundary layer (PBL i.e. through the top of model layer 2). Northern hemisphere summer and southern hemisphere winter are defined as April-September, and NH winter and SH summer are October-March. The upper part is for the 1850 case, and the lower part is for the 1990 case.

1850

Latitude	Net PO$_3$ in the *PBL* (Tg/6 months)		Net PO$_3$, in the *UT* (Tg/6 months)		Net upward flux from *PBL* (Tg/6 months)	
	Summer	Winter	Summer	Winter	Summer	Winter
90-32°N	49	9.9	4.9	-0.17	-56	-62
32°N-Equator	45	32	82	53	-8.7	-42
Equator-32°S	41	44	65	48	-27	-60
32-90°S	0.12	1.9	0.74	0.74	-30	-44

1990

Latitude	Net PO$_3$ in the *PBL* (Tg/6 months)		Net PO$_3$, in the *UT* (Tg/6 months)		Net upward flux from *PBL* (Tg/6 months)	
	Summer	Winter	Summer	Winter	Summer	Winter
90-32°N	176	25	83	21	-95	-114
32°N-Equator	149	154	189	152	31	-26
Equator-32°S	75	106	126	110	-32	-75
32-90°S	6.9	5.5	7.2	3.8	-37	-55

The largest change in chemical activity occurs over the industrialised regions at northern mid-latitudes. Table 4 shows the same ozone budget terms as in table 3 for 5 sectors during summer. The net ozone production increases the most in the boundary layer over North America and Europe, while there is no significant change in the marine boundary layer. In the upper troposphere there is a significant increase in net ozone production in all sectors due to transport of ozone precursors brough up by convection over the source regions. The net upward flux of ozone from te PBL, is negative for all regions. However, over North America the net downward flux decreases significantly in the 1990 case indicating that the number of gridcells and/or periods with positive upward flux from the PBL are increasing in the 1990 case.

Table 4. As table 3, but for northern hemisphere mid-latitude sectors (32°N-56°N). Pacific (147.5°E-132.5°W), North America (132.5°W-62.5°W), North Atlantic (62.5°W-12.5°W)m Europe (12.5°W-47.5°E), Asia (47.5°E-147.5°E).

Region	1850, April-Sept., (Tg/6 months)			1990, April-Sept., (Tg/6 months)		
	Net PO_3 PBL	Net PO_3 UT	Upward flux from PBL.	Net PO_3 PBL	Net PO_3 UT	Upward flux from PBL
Pacific	-0.8	-0.56	-5.2	-1.6	7.3	-9.5
N. America	11	0.97	-8.1	54	18	-2.5
N. Atlantic	-0.7	-0.95	-5.0	-0.6	8.5	-10
Europe	7.6	-0.22	-8.7	38	15	-17
Asia	19	5.7	-17	65	22	-28

4.2.4 Ozone in the boundary layer

In the boundary layer the ozone increase is most pronounced over the continental source regions (Figure 11a). The calculated concentrations in the 1850 case and the increase, 20-35 ppbv, are in good agreement with observations in Europe from the late 19th century (Volz and Kley, 1988) as well as with the present-day ozone concentrations (Logan, 1985; Oltmans and Levy, 1994). Figure 13 shows the seasonal cycle of calculated monthly averaged ozone mixing ratios during pre-industrial and present-day conditions for the grid box that includes Paris. Also shown are the observed concentrations from the Montsouris measurements (+) in the late 19th century and present day concentrations from the European background stations Arkona (asterisks) and Izpra (circles) (adopted from Anfossi et al., 1991). The observations from Montsouris were filtered to include only south westerly winds to avoid interference with local SO_2 pollution sources (Volz and Kley, 1988). This has not been done to the CTM data due to the coarse resolution of the CTM. The model gives pre-industrial ozone mixing ratios 2-3 ppbv higher than observed. The seasonal cycle for the pre-industrial times in both the observations and the CTM shows a maximum in late winter and early spring and a summer minimum. The summer minimum is caused by photochemical destruction mainly through reaction *R7* in the low NOx environment upwind of Paris (i.e. over the North Atlantic) in the 1850 case. The winter/spring maximum is probably caused by a seasonally enhanced intrusion of ozone rich air from the stratosphere.

In the 1990 experiment the seasonal cycle in the calculated ozone concentration changed dramatically with a pronounced summer maximum, in accordance with the observations. However, in the observations the concentrations start to increase somewhat earlier in spring. Since the upper boundary concentrations in the stratosphere were identical in both experiments, the calculated increase during spring is caused by photochemical production in the troposphere.

4.3 Changes in odd-hydrogen

Pollutants emitted to the atmosphere are transformed chemically to components that eventually are removed by deposition or scavenging by precipitation. For many of the key components in the troposphere, the initial and rate determining step in this process is oxidation by the hydroxyl radical (OH). Changes in the amount of OH could therefore have a significant influence on the concentrations of many important species in the troposphere.

The primary source of odd-hydrogen (OH+HO$_2$) in the atmosphere is the reaction of O(^{1}D), which is produced by photolysis of ozone (*R5*), with water vapour (*R6*). Odd-hydrogen is

eventually lost through formation of hydrogen peroxide (H_2O_2), which can be removed by washout and deposition, and through

$$OH + HO_2 \rightarrow H_2O + O_2 \hspace{4cm} R8$$
$$OH + NO_2 + M \rightarrow HNO_3 + M \hspace{3cm} R9$$

There is a rapid cycling of odd-hydrogen between the components within the odd-hydrogen family. Reactions of OH with CO and CH_4 gives HO_2, while reaction *R7* (background) and *R10* (polluted regions) transfers HO_2 back to OH.

$$NO + HO_2 \rightarrow NO_2 + OH \hspace{4cm} R10$$

The increased concentrations of ozone and NOx might lead to increased OH concentrations through reactions *R5, R6* and *R10*. (Isaksen and Hov, 1987; Fuglestvedt et al., 1996).

The increased levels of CH_4 have a dual role for HOx concentrations depending on the NOx concentrations. In low NOx background regions (NO< 5-10 pptv) oxidation of CH_4 leads to a loss of HOx, while HOx is produced at higher NOx levels (Crutzen, 1987; Cicerone and Oremland, 1988). The increase in the amounts of CO and CH_4 also leads to a shift in the partitioning within the HOx family, by decreasing the OH/HO_2 ratio, as OH is consumed in the initial steps, and HO_2 might be produced in the subsequent oxidation chain (Berntsen et al., 1992). Thus, in low NOx environments there has been a decrease in OH concentrations, while OH has increased in regions of the atmosphere where NOx is more abundant.

Table 5. Calculated seasonal and hemispheric mean concentrations of OH, HO_2 and H_2O_2 in the 1850 and 1990 case.

HOx-Species		NH		SH		Global
		Summer	Winter	Summer	Winter	Annual
OH	1850	13.0	6.1	11.0	6.1	9.03
(10^5 molec/cm^3)	1990	15.1	7.3	10.1	6.0	9.64
HO_2	1850	5.2	3.1	4.7	3.0	3.99
(10^7 molec/cm^3)	1990	7.6	4.5	6.3	3.9	5.58
H_2O_2	1850	2.7	1.8	2.4	1.7	2.16
(10^9 molec/cm^3)	1990	6.0	3.8	4.4	3.0	4.31

In these model experiments, the globally averaged OH concentrations given in Table 5 increased by 6 % from 1850 to 1990. The change is not spatially homogeneous. As discussed above, there is an increase of OH in NOx rich regions in the northern hemisphere (*R10*), while OH decreases in background regions, predominantly in the marine boundary layer and in the southern hemisphere. An important effect of this can be seen in Figure 14 which shows the global average lifetime (τ) of methane and CO and the relative changes in τ (i.e. $100 \times [\tau_{1990}-\tau_{1850}]/\tau_{1850}$) as a function of month. For both methane and CO, the relative change in lifetime is positive (decreased OH) during southern summer (October-April), and negative (increased OH) during northern summer (May-September). The difference is more pronounced for CO than for methane, due to its shorter lifetime and therefore the higher spatial correlation between the main region of CO oxidation and the region with enhanced OH concentrations.

In the polluted regions of northern mid-latitudes increased concentrations of ozone and NOx and increased oxidation of CH_4 in a 'high' NOx environment contribute to the increase in the OH levels in the 1990 case. In the less polluted regions of the southern hemisphere, low NOx

concentrations lead to increased destruction of both ozone and odd-hydrogen when methane and CO levels are increased in the 1990 case.
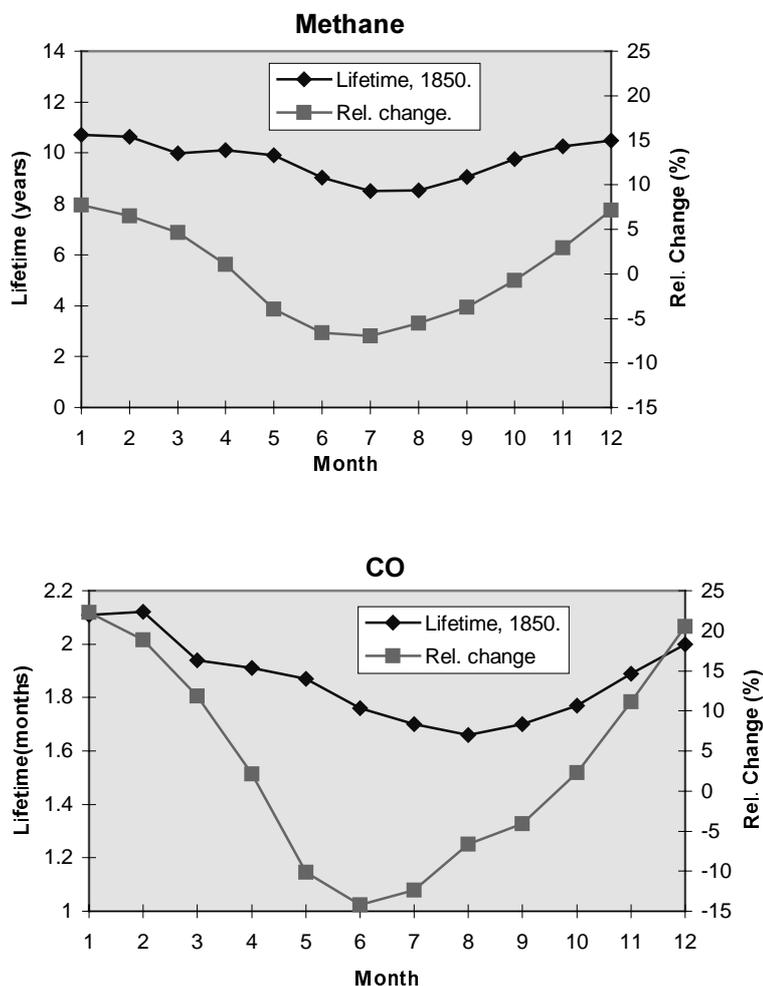

Figure 14. Seasonal cycle of globally averaged lifetime (τ) of methane and CO with respect to reaction with OH for the 1850 case. Also shown is the relative change τ given by
Rel. Change = 100x[τ_{1990}-τ_{1850}]/τ_{1850}.

The concentrations of the hydrogen peroxy radical HO_2 also change due to the changes in the emissions (Table 5). In contrast to the OH changes, HO_2 increases in both hemispheres and both seasons. In the southern hemisphere the increase is 30-35%, while in the northern hemisphere the increase is about 45% in both seasons. The reason for the stronger increase of HO_2 in the northern hemisphere is that in high NOx environments, the complete oxidation chain of methane produces about 3.5 molecules of HOx (Crutzen, 1987; Cicerone and Oremland 1988). In low NOx regions, radical-radical reactions like

$HO_2 + CH_3O_2 \rightarrow CH_3O_2H + O_2$ *R11*
$CH_3O_2 + CH_3O_2 \rightarrow CH_3O_2CH_3 + O_2$ *R12*
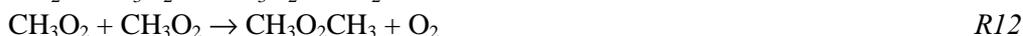
become more frequent, thereby allowing less production of HOx through methane oxidation.

The concentration of hydrogen peroxide increases even more than HO_2, due to the quadratic dependence of H_2O_2 production on HO_2 concentrations. Hydrogen peroxide is one of the major oxidants in cloud droplets. The increase in H_2O_2 concentrations could therefore have significant influence on the lifetime of SO_2.

The results from this study are in broad agreement with results from recent 3-D models (Crutzen and Zimmerman, 1991, Muller and Brasseur, 1995; Lelieveld and Dorland, 1995) which show small changes in the global mean OH-concentrations (less than 10% change, with regions with increases and decreases), but with significant increases in HO_2 and H_2O_2.

4.3.1 Implications for ozone

The general increase of HO_2 acts to decrease the lifetime of tropospheric ozone considerably in the present day atmosphere, as reaction *R7* is a very important loss mechanism for ozone in the troposphere. The calculated changes in ozone as given in Figures 10 and 11 are therefore the net result of increased production and decreased chemical lifetime since pre-industrial times. Assuming that reaction *R6, R7* and

$$O_3 + OH \rightarrow HO_2 + 2O_2 \hspace{3cm} R13$$

are the most important chemical loss mechanisms of ozone, the averaged weighted chemical lifetime of ozone in the troposphere can be approximated by the equation:

$$\tau = \overline{\left[\frac{\overline{O_3}}{(k_7 \times HO_2 + k_6 \times O(^1D) \times H_2O / O_3 + k_{13} \times OH) \times O_3} \right]}$$

where $\overline{X}$ denotes the global or hemispheric mean of X. The calculated lifetimes are given in Table 6. The global and annual averaged tropospheric lifetime of ozone decreased by 35% in the 1990 case.

Table 6. Approximate chemical lifetime of ozone in the troposphere for the 1850 and 1990 case

		Northern Hemisphere		Southern Hemisphere		Global mean
		Summer	Winter	Summer	Winter	
Lifetime O_3	1850	3.4	6.8	4.1	6.5	4.9
(Months)	1990	2.1	4.2	3.1	4.6	3.2

Night time nitrogen chemistry and heterogeneous reactions of N_2O_5 on deliquescent aerosols through the reactions

$$2(NO + O_3 \rightarrow NO_2 + O_2) \hspace{3cm} R14$$
$$NO_2 + O_3 \rightarrow NO_3 + O_2 \hspace{3cm} R15$$
$$NO_2 + NO_3 + M \rightarrow N_2O_5 + M \hspace{3cm} R16$$
$$N_2O_5 + H_2O \rightarrow 2HNO_3 \hspace{3cm} R17$$

also act to decrease the lifetime of ozone, in particular in the northern hemisphere during winter. Three molecules of ozone are lost when two NOx molecules are oxidized to HNO_3. Due to the quadratic dependence of the N_2O_5 formation on the NOx concentrations (reaction *R16*) and the lower aerosol content, this process had a negligible influence during pre-industrial times. Increased levels of NOx since 1850 therefore also act to decrease the lifetime

of ozone. Dentener and Crutzen (1993) calculate in a 3-D CTM that between 20 and 80% of the NOX loss ($NOX=NO+NO_2+NO_3+2N_2O_5+PAN+HNO_4$) is through reactions on aerosols. Assuming a loss of 50% (or about 20 Tg(N)/yr) leads to an additional loss of ozone of 100 Tg/yr of ozone, or about 10% compared with the estimated present surface deposition of ozone (Table 2).

5. Radiative forcing

The calculated changes in tropospheric ozone due to increased emissions between 1850 and 1990 discussed in Section 3 and 4, have been used in two different radiative transfer models to calculate the radiative forcing.

5.1 Input and procedures in radiation modelling

Temperatures and humidities were in both models largely derived from ECMWF analyses, in Reading averaged over the period 1980-1991, in OsloRad over the years 1992-1994. In the Reading model some modifications of ECMWF data were introduced. In the upper stratosphere, temperatures were derived from Fleming et al. (1990). At pressures less than 300 hPa, the water vapour climatology was based on a first-guess field used in Microwave Limb Sounder retrievals and was provided by H.C.Pumphrey (Univ of Edinburgh, personal communication). It is largely based on SAGE II and HALOE data. Cloud amounts and optical depths in both models were seven-year averages from ISCCP (Rossow and Schiffer, 1991); clouds were specified at three levels in the atmosphere. The surface albedos were also taken from ISCCP data. In addition to water vapour and clouds, the thermal infrared calculations include the absorption by nitrous oxide, methane and carbon dioxide; the effect of overlap with these species is small (less than 5%) as the main absorption band of ozone (at 9.6 μm) is well away from the strongest absorption bands of these gases.

Ozone data are taken from different sources in the Reading and OsloRad models. In the OsloRad model the tropospheric ozone values calculated with the CTM in the 1850 and in the 1990 cases are used directly in the calculations, and in the stratosphere the ozone data are taken from Liang and Wang (1995). A different approach was taken in the Reading calculations where present day ozone data were taken from an observed climatology derived by Li and Shine (1995). This was largely based on SBUV and SAGE II data for the period 1985-1989. At pressures greater than 100 hPa, the column ozone is derived as a difference between TOMS total ozone and the column between 0 and 100 hPa derived from the SBUV and SAGE data. The shape of the vertical profile in the troposphere was specified from ozonesondes. The ozone data used for pre-industrial calculations in the Reading model were calculated by subtracting the absolute changes computed in the CTM from pre-industrial to present time, from the present day observed climatology.

The radiative forcing was calculated for both clear and cloudy skies and including and excluding the adjustment of stratospheric temperatures. An increase in tropospheric ozone leads to a reduction in the upwelling thermal infrared irradiance reaching the lower stratosphere (and, to a much smaller extent, there is a reduction in the reflected shortwave radiation) which acts to cool the stratosphere (see e.g. Ramaswamy and Bowen 1994). This cooling reduces the thermal infrared emission from the stratosphere which reduces the energy available for the surface-troposphere system; since this cooling takes place on a time-scale of a few months, compared to the decadal time-scale of the surface temperature response, it is often taken to be part of the forcing (see e.g. IPCC 1994). When the stratospheric temperature change is included, the forcing is referred to as "adjusted"; otherwise it is referred to as "instantaneous".

The fixed-dynamical-heating approximation is used to calculate the stratospheric temperature adjustment (see e.g. Ramanathan and Dickinson 1979). Before the ozone is perturbed, the net radiative heating at each level in the stratosphere, and at each grid point, is assumed to be balanced by a dynamical heating of the opposite sign. On perturbing the tropospheric ozone,

this dynamical heating is assumed to be fixed and a new stratospheric temperature profile is found, by iteration, for which the radiative heating exactly balances the dynamical heating.

5.2 Global and hemispheric averages

The annual and global mean radiative forcing due to the change in tropospheric ozone from pre-industrial to present time, from the Reading and OsloRad models, are shown in Table 5. Several cases have been run including instantaneous as well as adjusted forcing under clear and cloudy conditions. Many of the basic features have been discussed elsewhere (e.g. Wang et al., 1993; Hauglustaine et al., 1994; Forster et al., 1997). The increase in tropospheric ozone leads to a positive forcing due to an increased absorption of both thermal infrared and solar radiation (in contrast to the effect of stratospheric ozone changes where the solar and thermal infrared forcings oppose each other). The effect of clouds is a reduction in the thermal infrared forcing, due to the increased opacity of the troposphere, but an increase in the solar forcing, due to the additional absorption of photons reflected by low clouds in particular. The adjustment of stratospheric temperatures causes almost no change in the solar forcing but causes a large decrease in the thermal infrared as a result of the stratosphere cooling.

The cloudy sky adjusted forcing is felt to be the most appropriate indicator of climate response (e.g. IPCC, 1994; Hansen et al., 1997). As was highlighted by Forster et al. (1997), the difference between the net forcing in the cloudy sky adjusted case and the other cases is significant. Sometimes other authors have used one of the other cases to describe the ozone radiative forcing. In the annual mean, neglect of cloud leads to an overestimate of the net forcing by 20% in both the instantaneous and adjusted case. The neglect of adjustment leads to an overestimate of between 20 and 30%. Neglect of both clouds and stratospheric adjustment leads to an overestimate of more than 50%. It is also notable that in the Reading cloudy adjusted case, the solar forcing contributes 27% of the total forcing, whereas in the clear sky instantaneous case, it contributes only 13%.

Table 5: Global mean and annual mean radiative forcing due to the change in tropospheric ozone from pre-industrial to the present time from the Reading and OsloRad models. The instantaneous forcing for both clear and cloudy skies and the forcing when stratospheric temperatures are adjusted, for both clear and cloudy skies, are shown. LW is the thermal infrared forcing, SW is the solar forcing and Net is the sum of these. Notice that the shortwave results for the OsloRad model are without clouds in all cases. All values are given in Wm^{-2}.

			Net		LW		SW	
			Reading	OsloRad	Reading	OsloRad	Reading	OsloRad
Global	Instant.	Clear	0.40	0.48	0.35	0.42	0.05	0.06
Global	Instant.	Cloudy	0.33	0.36*	0.26	0.30	0.07	
Global	Adjusted	Clear	0.31	0.39	0.26	0.33	0.05	0.06
Global	Adjusted	Cloudy	0.26	0.29*	0.19	0.23	0.07	

(*) Without clouds in SW calculations

The absolute reduction in the thermal infrared forcing between the instantaneous and adjusted cases is identical in the Reading and OsloRad models, although it is a slightly greater percentage in the Reading case. It has been estimated that the temperature adjustment is largely due to the change in the upwelling thermal infrared radiation (94%) and only to a small extent by the change in reflection of the shortwave radiation (6%). The effect of clouds on the thermal infrared forcing is greater in the OsloRad model in both absolute and percentage terms; in the adjusted case the clear/cloudy ratio is 1.43 for OsloRad and 1.37 for Reading. The clear sky shortwave forcings differ by 16% presumably due to different surface albedos and different methods of calculating the diurnal-mean solar radiation.

Table 6 shows the cloudy-sky adjusted forcing for the two hemispheres as calculated by the two models. Each component is at least 70% greater in the northern hemisphere than in the southern hemisphere due to the much larger change in ozone in the northern hemisphere.

Table 6: Hemispheric and global annual mean radiative forcing (in Wm^{-2}) for the cloudy-sky adjusted case using the Reading and the OsloRad models. Notice that clouds are included in all calculations except the shortwave calculation of the OsloRad model.

			Net		LW		SW	
			Reading	OsloRad	Reading	OsloRad	Reading	OsloRad
Global	Adjusted	Cloudy	0.26	0.29*	0.19	0.23	0.07	0.06*
NH	Adjusted	Cloudy	0.33	0.37*	0.24	0.30	0.09	0.08*
SH	Adjusted	Cloudy	0.19	0.21*	0.14	0.17	0.05	0.04*

(*) Without clouds in SW calculations

The global and annual mean radiative forcing from OsloRad (0.29 Wm^{-2}) and Reading (0.26 Wm^{-2}) agree very well but this is to some extent coincidental. The Reading thermal infrared forcing is significantly lower (at 0.19 Wm^{-2}) than the OsloRad forcing (at 0.23 Wm^{-2}) but this is compensated by the fact that the Reading shortwave forcing includes clouds, whereas the OsloRad values do not. Including clouds in the shortwave causes the Reading forcings to be higher by 0.02 Wm^{-2}.

The offset between the OsloRad and Reading thermal infrared results appear little affected by the inclusion of clouds and stratospheric adjustment. The OsloRad thermal infrared forcing is typically 20% higher than Reading in all cases. The spatial patterns of the forcing show generally good agreement (see Section 5.3). It is also known that the two sets of radiation schemes agree to within a few percent when the tropospheric ozone changes specified in a model intercomparison (Shine et al 1995) are used (see Section 2.2). The prime cause of the difference appears to be due to how the ozone perturbations are applied in the models. OsloRad calculated the forcing using the pre-industrial and present day ozone fields supplied from the chemical model. Reading used the absolute changes in ozone from the chemical model and imposed these on the observationally-based ozone distribution described in Section (5.1). A trial calculation of the instantaneous clear sky forcing for July was performed with the Reading model using the OsloRad method and it was found that the thermal infrared forcing increased from 0.36 Wm^{-2} to 0.44 Wm^{-2}, similar to the value obtained in the OsloRad model whilst the solar forcing was unchanged. The 20% increase in thermal infrared forcing accounts for much of the difference between the two models. These calculations indicate that differences in the representation of the present-day ozone field lead to a quite significant unertainty in the value of forcing and emphasise the need for more tropospheric ozone data to help evaluate models.

In the results presented above, the calculations in the chemistry model are performed up to about 100 hPa. In one experiment the chemistry model performed similar calculations only up to about 200 hPa. At low latitudes this is lower than the tropopause height which is normally around 100 hPa in this region. The instantaneous thermal infrared radiative forcing was reduced from 0.30 Wm^{-2} to 0.18 Wm^{-2} in the OsloRad model. This difference occurs in the latitudinal region 30°S to 30°N where the tropopause level is above 200 hPa. This result indicates the importance of upper tropospheric ozone changes.

5.3 Geographical patterns

Figures 15 and 16 show the annual-mean geographical distribution of the cloudy sky adjusted forcing for the shortwave, the thermal infrared and the net calculated with the Reading and OsloRad models, respectively. The pattern of forcing strongly resembles the pattern of the change in total tropospheric column ozone, as is shown in Figure 12, but it is also affected by a number of other factors such as the distribution of temperature and cloudiness. The minima near the equator are mainly a result of the distribution of column ozone change which peaks north of the equator in January, April and July but has a strong peak south of the Equator off the west coast of Africa, in October; it is also partially due to the equatorial maxima in the high cloud amount. In the clear sky forcing (not shown) there is a much smaller decrease with latitude in the thermal infrared forcing polewards of the northern subtropics than is found for the cloudy cases.

The shortwave radiative forcing from the Reading model shows a large hemispheric difference; however in each hemisphere the spatial distribution of the radiative forcing is relatively homogeneous. The peak value is over the Saharan and Arabian deserts, and at high northern latitudes there is a somewhat smaller peak. The spatial pattern in the shortwave radiative forcing from the OsloRad model differs substantially from the shortwave forcing in the Reading model, mainly because clouds are not included in the OsloRad model. The peak values are larger over the high albedo areas in the OsloRad model partly due to higher horizontal resolution and also probably due to higher albedo in some of the high albedo areas.

The thermal infrared forcing shows a much greater spatial variation than the Reading shortwave forcing, with a strong peak in the northern subtropics, especially over the Saharan and Arabian deserts. The location of the peak is very similar as for the shortwave forcing, however, the gradients and contrasts are much stronger for the thermal infrared forcing. The thermal infrared radiative forcing is generally higher in the OsloRad model than in the Reading model due to the higher background concentration of tropospheric ozone in the Reading model. The difference is most pronounced over areas with small cloud amounts, because the background concentration of tropospheric ozone is more important for clear sky conditions than for cloudy conditions, and that clouds reduce the thermal infrared radiative forcing more in the OsloRad model than in the Reading model as seen in Table 5.

In order to help understand the factors that cause the regional distribution of forcing, an additional calculation was performed using the Reading model in which the ozone was perturbed by 10 ppbv everywhere in the troposphere. The annual-mean cloudy sky adjusted forcing is shown in Figure 17.

The thermal infrared forcing (Figure 17(a)) shows peaks over areas that have both generally clear skies and high surface temperatures, most notably over north Africa and the eastern tropical Pacific. There is a general fall off in forcing with latitude, due to the decrease in surface temperature, the general increase in cloud amount and the decrease in the depth of the troposphere. There are marked minima in equatorial regions, over south America, central Africa

and Indonesia, coinciding with the regions of deep convection and, hence, large amounts of high cloud. Comparison with the forcing derived from the modelled ozone changes (Fig 15(a)) shows that the peak in forcing over north Africa is due to a coincidence of regions with substantial ozone change with regions where the ozone is, radiatively, most effective. The minima along the equator are similarly due to a coincidence of generally lower ozone change and lower effectiveness.

The shortwave forcing following the 10 ppbv change (Fig 17(b)) shows much structure. Maxima occur over regions of extensive low cloud (such as the stratocumulus on the eastern side of the sub-tropical oceans) and over areas of high surface albedo (such as deserts, snow and ice). This is because the solar radiation is absorbed by the extra 10 ppbv ozone in both its downward and upward passage through the atmosphere. The presence of high clouds, especially over south America, central Africa and Indonesia, reduces the impact of the added ozone because the high cloud shields the lower troposphere; there is a lower amount of solar radiation to be absorbed by the extra ozone. The effect of surface albedo is also noticeable because of the relative minimum in effectiveness in mid-latitudes where surface albedos are lower, compared with high latitudes, despite the decrease in the annual-mean insolation with latitude. The large cloud amounts in the storm tracks also contribute to this modulation. The shortwave forcing derived from the modelled ozone changes (Figure 15(b)) shows less structure. The region of high effectiveness over north Africa is coincident with the region of substantial ozone change. There is less difference between mid and high latitudes because the increased effectiveness of the high latitude ozone change is offset by the smaller ozone changes there.

In low latitudes, the effect of high clouds and the effect of desert regions (which have generally clear skies, high surface albedos and high surface temperatures) tend to cause regions of high radiative effectiveness to coincide in both the shortwave and thermal infrared; hence the effects reinforce each other in the net forcing following the 10 ppbv change (Figure 17(c)). The poleward decrease in forcing in the extratropics in the thermal infrared is compensated by the shortwave effects to give a lower latitudinal gradient in the net forcing.

Considering the thermal infrared and shortwave forcing from the actual ozone change (Fig 15) the weaker pattern in the shortwave forcing arises because the shortwave forcing is strongly determined by both the change in column ozone <u>and</u> the distribution of insolation. Thus, whilst in the near-equinoctial months (not shown), the distribution of forcing closely resembles the pattern of ozone change, in the near-solstice months the distribution is strongly modulated by the available insolation. For example in January, the shortwave forcing is only a factor of two higher over the Arabian Sea compared to the southern tip of South America, whilst the thermal infrared is a factor of 9 higher.

One interesting but somewhat incidental aspect of the Reading calculation in which the ozone is perturbed by 10 ppbv everywhere in the troposphere, is that the global and annual mean net forcing of 0.2 Wm^{-2} is in very good agreement with the very simple parameterisation suggested by IPCC (1990) (and as used by Marenco et al.(1994)), where the forcing was equal to 0.02 $Wm^{-2}ppbv^{-1}$. Hence this simple expression provides a useful means for first-order estimates of the forcing due to tropospheric ozone change.

To examine the dependence of the forcing on details of the pattern of ozone change, cloudiness etc., the forcing calculations were repeated using the zonally-averaged fields for both the climatology and the ozone changes. The forcing was found to agree with the longitudinally-resolved forcing to within 5% at each latitude. The relative contribution from shortwave and the thermal infrared forcings were of similar magnitude. The global mean thermal infrared radiative forcing using zonally-averaged fields of input data was found to deviate by less than 1% from the radiative forcing when the longitudinal variation of the input

data was included. This is similar to the results of the case of well-mixed greenhouse gases in Myhre and Stordal (1997). Many of the previous assessments of ozone radiative forcing have been performed using zonal-mean analyses. Thus whilst the computation of the ozone change using a 2-D model may be different to that calculated using a 3-D model, the calculation of the forcing is only modestly affected by the zonal averaging. This also indicates that the zonal average of output from 3-D chemical transport models could be used to approximate the ozone radiative forcing.

5.4 Seasonal variation

There is a significant seasonal cycle in the calculated forcing. This is shown in Figure 18, which includes results for thermal infrared, shortwave, and net forcing from the OsloRad model. The seasonal variation is first of all due to the seasonal cycle in the global-mean changes in the total tropospheric ozone, which varies from 5.7 Dobson Units (DU) in February to 8.4 DU in October in the OsloRad model. This 47% increase in ozone is matched by a 43% increase in the net cloudy adjusted forcing in the OsloRad model. The yearly average net forcing in the OsloRad model calculated based on the 4 selected months used by Reading deviated from the averaged based on all the 12 months by less than 1%.

The seasonal cycle in the net forcing is mostly influenced by the cycle in the thermal infrared, which in turn is seen to be influenced by variations in the radiative forcing in both hemispheres and maximizes in the September to October period. There is a high thermal infrared radiative forcing in the southern hemisphere in this period which is mainly due to biomass burning which gives a significant ozone increase at high altitudes in the troposphere. In both hemispheres there is a large yearly variation in the shortwave radiative forcing. During fall and early winter in the Northern hemisphere the shortwave radiative forcing is about equal in the two hemispheres. The global shortwave radiative forcing is largest in May.

5.5 Stratospheric Temperature Changes due to Tropospheric Ozone Increases

In this section we briefly present the model-predicted changes in stratospheric temperature as a consequence of the tropospheric ozone increase. There is considerable evidence for the long-term cooling of the stratosphere (e.g. WMO, 1994; Ramaswamy et al., 1996). Although changes in *stratospheric* ozone loss seem likely to be a major cause of these changes, there are many other potential mechanisms, such as changes in carbon dioxide and stratospheric water vapour (see e.g. Ramaswamy et al., 1996; Forster and Shine, 1997). Ramaswamy and Bowen (1994) have drawn attention to the possible effects of changes in tropospheric constituents on stratospheric temperatures and have shown that, on a global mean, a 50% increase in tropospheric ozone may lead to a cooling of about 0.2 K at an altitude of 23 km.

Figure 19 shows the stratospheric cooling, using the fixed dynamical heating approximation, and the ozone changes from the CTM. The calculations are for July and are from the Reading model. The sub-tropical northern hemispheric cooling reaches 0.68 K at about 20 km, and is more than 0.1 K over much of the lower stratosphere north of 40°S. The pattern is qualitatively similar for the other mid-season months and the cooling exceeds 0.9 K at 15°N lower stratosphere in April. It must be recalled that the fixed dynamical heating changes are only approximate and the temperature patterns derived from a GCM might be significantly different (see e.g. Boville and Kiehl, 1988).

These values of cooling are substantial, as typical observed stratospheric coolings are a few tenths of a degree per decade (e.g. WMO, 1994). The coolings due to stratospheric ozone change over the period 1979-1990 calculated using a GCM by Ramaswamy et al. (1996) are about 0.5 K in the equatorial lower stratosphere and exceed 1 K in the northern hemisphere extratropical lower stratosphere (although the exact pattern depends markedly on assumptions about the horizontal and vertical ozone change - see Forster and Shine (1997)).

One difficulty in placing the coolings from the tropospheric ozone change in context is that they relate to the entire period since pre-industrial times, and would represent a relatively slow rate of cooling if averaged over more than a century. Trend analysis of the ozonesonde measurements from Payerne, Switzerland, (Staehelin and Schmid, 1991) and of the Pic de Midi data series (Marenco et al., 1994) indicate that there has been an increase in the free tropospheric ozone concentrations at northern mid-latitudes of the order of 30 % (15-20 ppbv), during the 1967-1990 period. The increase now seems to have stopped over Europe and north America, while there appears to be a positive trend over East Asia (Logan, 1994). Comparing the observed trends with the calculated increase (Figure 10 and 11), it appears that about 50 % of the increase has occurred since the 1950s. If half of the total change shown in Figure 19 occurred in 40 years, there are still some regions where the cooling exceeds 0.05K/decade; hence the role of tropospheric ozone is not negligible.

6. Comparison with previous work

A number of recent studies have reported estimates of the global radiative forcing due to tropospheric ozone change. These are listed in Table 9. Hauglustaine et al. (1994) used a 2-D chemical transport model - their value does not appear to include the effect of stratospheric adjustment; Marenco et al (1994) used historical observations of surface ozone and modern observations of the interhemispheric difference in ozone concentration, along with a simple parameterisation of the dependence of radiative forcing on ozone change; Lelieveld and van Dorland (1995) used a 3-D chemical transport model and calculated the clear sky adjusted forcing; Chalita et al. (1996) calculated the instantaneous cloudy sky forcing using ozone changes from a 3-D model. Forster et al. (1997) calculated the adjusted cloudy-sky forcing using ozone changes from two different 2-D models.

There are many potential reasons for differences in the results. Assumptions about the changes in (and distribution of) pre-cursor emissions, the chemistry included and the transport by advection and convection are quite different in the CTMs. The model based estimates of pre-industrial tropospheric ozone burdens range from 151 to 380 Tg, while for present day conditions the range of the estimates are 250 to 550 Tg (Table 9). The estimated changes in in the tropospheric ozone burden presented in this paper compare very well with the results from Lelieveld and van Dorland (1995), although our estimates are 15-20% higher during both periods. Also the radiation schemes and the methodology used to derive the forcing differ. The present calculations are much closer to the Forster et al. (1997) calculations using the UK Meteorological Office (UKMO) 2-D model ozone changes, than using the Univ. of Cambridge (CAMB) 2-D model; this is largely due to the column ozone changes being closer to the UKMO values than the CAMB values, which were typically 40% higher. Marenco et al. (1994) assumed that the pre-industrial ozone concentration was 10 ppbv throughout the troposphere, which is likely to be an extreme assumption.

The Lelieveld and van Dorland value could, using the figures from Table 9, be reduced by about 20% to account for the effect of clouds, as could the Hauglustaine et al. and Chalita et al. values to account for the effect of stratospheric temperature adjustment. On making these adjustments all the model-based forcing estimates range from about 0.22 to 0.5 Wm^{-2} which indicates that a substantial amount of the disagreement is due to the differences in the predicted ozone change; this supports the conclusion of Forster et al. (1997) who used the ozone change from two different models in the same radiation scheme, and found a similar range.

Table 9. Estimates of changes in tropospheric ozone and its radiative forcing. A comparison of values presented in this paper with other work for the hemispheric and global means (in Wm⁻ and the ratio of the northern and southern hemisphere forcing. See text for more details on the individual calculations. n.a.: not available.

	Trop. ozone burden (Tg)		Radiative Forcing (W/m^2)			
	1850	1990	Northern Hemisph.	Southern Hemisph.	Global	Ratio of Northern to Southern
Hauglustaine et al., 1994	n.a.	250			0.55	
Marenco et al, 1994	80[**]	330[**]	0.88	0.36	0.62	2.4
Chalita et al, 1996	n.a.	n.a.	0.40	0.17	0.28	2.4
Lelieveld and van Dorland, 1995	151	253			0.50	
Forster et al (1997b)-CAMB[*]	380	549	0.61	0.42	0.51	1.5
Forster et al 1997b- UKMO	223[*]	325[*]	0.35	0.24	0.30	1.5
Present Paper - OsloRad	192	294	0.37	0.20	0.28	1.9
Present Paper - Reading[*]	192[*]	294[*]	0.33	0.19	0.26	1.7

[*]Tropospheric ozone burdens are from the CTMs. In the calculations of the radiative forcing, the 1990 values were fixed to an ozone climatology, and only the ozone changes from the CTMs were used.
[**]Trop. ozone burdens infered from the assumptions given in Marenco et al. (1994) on mean tropospheric mixing ratios of ozone.

7. Conclusions

Changes in the concentrations of ozone in the troposphere since 1850 due to increased emissions of NOx, CO and CH_4, have been calculated with a global 3-D CTM. Significant increases in the amount of ozone are found, in particular in the upper troposphere. Increased *in-situ* production in this region due to enhanced vertical transport of precursors from the boundary layer and emissions from aircraft are found to be the major causes for the increase. The concentrations of the hydroxyl radical, OH, are found to have increased by 6%, while the global mean HO_2 concentrations have increased by 40 %. This increase is found to have significant impact on the chemical lifetime of ozone in the troposphere, which decreased by 35 % (global, annual, weighted mean). The calculated change in ozone concentrations have been used as input to two radiative transfer models to calculate the radiative forcing.

The global and annual mean radiative forcing due to the change in tropospheric ozone as calculated with the CTM are 0.26 and 0.29 Wm^{-2} in the Reading and OsloRad models respectively. Clouds are not included in the shortwave calculation in the OsloRad model, which in the Reading model increase the forcing by 0.02 Wm^{-2}. It is shown that the radiative forcing due to change in tropospheric ozone is dependent upon the background concentration of the tropospheric ozone, and this explains most of the difference between the calculated radiative forcing in the two models. The calculated radiative forcing in this work is in the lower range of previous estimates and the estimate in IPCC (1994). The inclusion of clouds and the stratospheric temperature adjustment reduce the radiative forcing; however, in some previous studies these have been neglected leading to larger values than in this study.

The regional, seasonal, as well as the hemispheric differences in the radiative forcing due to changes in tropospheric ozone are higher than the corresponding differences in the radiative forcing due to changes in the concentration of a well-mixed greenhouse gases see e.g. Myhre and Stordal (1997). This implies that changes in tropospheric ozone may give a different dynamic response and thus a different climate change, than changes in well mixed greenhouse gases (Wang et al., 1995). Detailed experiments with a general circulation model are required to establish the extent of the difference.

Given that the radiative forcing due to changes in the concentrations of carbon dioxide, methane, nitrous oxide and the CFCs since pre-industrial times is about 2.5 Wm^{-2} (IPCC 1995), the tropospheric ozone change over the same period causes, even at the lower limit, about 10% of the well-mixed greenhouse gas forcing; the contribution could be as high as 20%, at which point tropospheric ozone would become a more important contributor to the radiative forcing than the direct effect of methane itself. The increase of methane is of course also one of the main reasons for the increase in tropospheric ozone. The effect of tropospheric ozone change on stratospheric temperature have also been shown to be potentially significant.

A related issue is the relative size of the tropospheric ozone forcing compared to the effects of sulphate aerosols - several GCM studies have included the direct effects of aerosol forcing in transient climate change experiments, but neglected the contribution of tropospheric ozone changes (see IPCC 1995). The latest IPCC (1995) estimate of the sulphate aerosol forcing is - 0.4 Wm^{-2} with a factor of two uncertainty, indicating that tropospheric ozone change is around the same size as, but of the opposite sign to the sulphate aerosol effect. In addition, the interhemispheric difference in the sulphate forcing has been used in detection studies (see IPCC 1995). A typical value for the ratio of the northern/southern hemisphere forcing for sulphate aerosol is 3 or 4 - the ratio for the ozone change is somewhat less (between 1.5 and 2 - see Table 9) but this is nevertheless a significant offset to the interhemispheric contrast that may have been caused by the sulphate aerosol.

All these factors serve to emphasise that despite the remaining uncertainties, tropospheric ozone change appears to be a very significant contributor to the total radiative forcing due to human activity. The forcing due to changes in carbon dioxide is the only forcing that is clearly larger than the effect of tropospheric ozone change; the highly uncertain forcing due to aerosol-induced changes in cloud albedo (e.g. IPCC 1995) may also be larger. The effect of more recent stratospheric ozone loss appears smaller than the effect of tropospheric ozone (IPCC 1995; Forster and Shine, 1997; Myhre et al., 1996) although the upper limit calculated by Forster and Shine (-0.25 Wm^{-2}) for the effect of stratospheric ozone change since about 1960 is similar to the lower limit of the positive forcing caused by tropospheric ozone since pre-industrial times.

Acknowledgement

References

Anfossi D., S. Sandroni and S. Viarengo. Tropospheric ozone in the nineteenth century: The Moncalieri series. *J. Geoph. Res.*, **96**, 17349-17352, 1991.

Bekki, S., Law, K.S. and Pyle, J.A. Effect of ozone depletion on atmospheric CH_4 and CO concentrations. *Nature*, **371**, 595-597, 1994.

Berntsen T., J.S. Fuglestvedt and I.S.A. Isaksen. Chemical-dynamical modelling of the atmosphere with emphasis on the methane oxidation. *Ber. Bunsenges. Phys. Chem.*, **96**, pp 241-251, 1992.

Berntsen T., I.S.A. Isaksen, W.-C. Wang and X.-Z. Liang. Impacts of increased anthropogenic emissions in Asia on tropospheric ozone and climate: A global 3-D model study. *Tellus,* **48B,** 13-32, 1996.

Berntsen T. and I.S.A. Isaksen. A global 3-D chemical transport model for the troposphere;1. Model description and CO and ozone results. Submitted to *J. Geoph. Res.,1997*

Borrman S., S. Solomon, J.E. Walters and B. Luo. The potential of cirrus clouds for heterogeneous chlorine activation. *Geophys.Res.Lett.,* **23,** 2133-2136, 1996.

Boville B.A., and J.T. Kiehl. The radiative-dynamical response to of a stratospheric-tropsopheric general circulation model to changes in ozone. *J. Atmos. Sci.*, **45**, 1798-1817, 1988.

Brasseur G.P, D.A Hauglustaine and S. Walters. Chemical compounds in the remote Pacific troposphere: Comparison between MLOPEX measurements and transport model calculations. *J. Geoph. Res*., **101**, 14795-14813, 1996.

Chalita S., D.A. Hauglustaine, H.Le Treut and J-F. Müller. Radiative forcing due to increased tropospheric ozone concentrations. *Atmos.Environ.,* **30,** 1641-1646, 1996.

Cicerone R.J. and R.S. Oremland. Biogeochemical aspects of atmospheric methane. *Global Biogeochemical Cycles*, **2**, 299-327, 1988.

Cox, S.J., W-C.Wang and S.E.Schwartz. Climate response to forcings by sulphate aerosols and greenhouse gases. *Geophys.Res.Lett.,* **18,** 2509-2512, 1995.

Crawford J., D.Davis, G.Chen, J.Bradshaw, S.Sandholm, G.Gregory, G.Sachse, B.Anderson, J.Collins, D.Blake, H.Singh, B.Heikes, R.Talbot and J.Rodriguez. Photostationary state analysis of the NO_2-NO system based on airborne observations from the western and central North Pacific. *J. Geoph. Res*., **101**, 2053-2072, 1996.

Crosley D. NO_y Blue Ribbon panel. *J. Geoph. Res*., **101**, 2049-2052, 1996.

Crutzen P.J. Role of the tropics in atmospheric chemistry. In *The geophysiology of Amazonia*, Ed. by R.E. Dickinson, pp 107-130, John Wiley, New York, 1987.

Crutzen P.J. and P.H. Zimmermann. The changing photochemistry of the troposphere. *Tellus,* **43AB**, 136-151, 1991.

Dentener F. and P.J.Crutzen. Reaction of N_2O_5 on tropospheric aerosols: Impact on the global distributions of NOx, O_3 and OH. *J. Geoph. Res.*, **98**, 7149-7163, 1993.

Fehsenfeldt F.C. and S.C. Liu. Tropospheric ozone: Distribution and sources. In *Global Atmospheric Chemical Change* (ed. C.N. Hewitt and W.T. Sturges). Elsevier Science Publishing Co., Inc., New York, 1993.

Fleming, E.L., S.Chandra, J.J.Barnett and M.Corney. Zonal mean temperature pressure, zonal winds and geopotential height as a function of latitude. *Adv. Space Res.,* **10,** (12)11-(12)59, 1990.

Forster, P.M.de F. and K.P.Shine. Radiative forcing and temperature trends from stratospheric ozone depletion. *J.Geophys.Res.,* (to appear) 1997a

Forster, P.M.de F., C.E.Johnson, K.S.Law, J.A.Pyle and K.P.Shine. Further estimates of radiative forcing due to tropospheric ozone changes. *Geophys.Res.Lett., (to appear) 1997b*.

Fuglestvedt, J.S., J.E. Jonson and I.S.A. Isaksen.Effects of reductions in stratospheric ozone on tropospheric chemistry through changes in photolysis rates. *Tellus*, **46B**, 172-192, 1994.

Fuglestvedt, J.S., Jonson, J.E., Wang, W.-C. and Isaksen, I.S.A. Responses in tropospheric chemistry to changes in UV fluxes, temperatures and water vapour densities. In: *Atmospheric Ozone as a Climate Gas*, Wang, W.-C. and Isaksen, I.S.A. (Eds.). Springer, 145-162, 1995.

Fuglestvedt, J.S., Isaksen, I.S.A. and Wang, W.-C. Estimates of Indirect Global Warming Potentials for CH_4, CO and NO_X. *Climatic Change*, **34**, 405-437, 1996.

Hansen, J., M.Sato, and R.Ruedy. Radiative forcing and climate response. *J.Geophys.Res.,* **102,** 6831-6864, 1997.

Haugland S.O. Mid-latitude stratospheric-tropospheric ozone exchange - a trend study. In *Atmospheric ozone as a climate gas*. (ed.W.-C. Wang and Isaksen I.S.A.). NATO ASI Series I, **32**, 181-187, Springer Verlag, 1995.

Hauglustaine, DA., C.Granier, G.P.Brasseur and G.Megie. The importance of atmospheric chemistry in the calculation of radiative forcing on the climate system. *J.Geophys.Res.,* **99,** 1173-1186, 1994.

Hauglustaine D.A., B.A. Ridley, S. Solomon, P.G. Hess and S. Madronich. HNO_3/NOx ratio in the remote troposphere during MLOPEX 2: Evidence for nitric acid reduction on carbonaceous aerosols? *Geophys.Res.Lett.,* **23,** 2609-2612, 1996.

Hesstvedt E., Ø. Hov and I.S.A. Isaksen. Quasi steady-state approximation in air pollution modelling: Comparison of two numerical schemes for oxidant prediction. *Int. Journal of Chem. Kinetics*, **X**, 971-994, 1978.

IPCC 1990. Climate Change. Cambridge University Press.

IPCC 1994. Climate Change 1994. Cambridge University Press.

IPCC 1995. Climate Change 1995. Cambridge University Press

Isaksen I.S.A., K.H. Midtbø , J. Sunde and P. Crutzen. A simplified method to include molecular scattering and reflection in calculations of photon fluxes and photodissociation rates. *Geophysica Norvegica,* **31**, No. 3, 1977.

Isaksen I.S.A., Ø. Hov and E. Hesstvedt. Ozone generation over rural areas. *Envir. Sci. Tech.,* **12,** 1279-1284, 1978

Isaksen I.S.A. and Ø. Hov. Calculations of trends in the tropospheric concentrations of O_3, OH, CO, CH_4 and NOx. *Tellus*, **39B**, 271-283, 1987.

Jacobs D. et al.. Evaluation and intercomparison of global atmospheric models using [222]Rn and other short lived species. *J. Geoph. Res*, **102,** 5953-5970. 1997.

Jaffe D., T.Berntsen and I.S.A.Isaksen. A global 3-D chemical transport model for the troposphere; 2. Nitrogen oxides and non methane hydrocarbons. Accepted for publication in *J. Geoph. Res. 1997.*

Jonson J.E., Model calculations of cloud processes and tropospheric ozone in the northern mid-latitudes. *PhD-thesis presented at the University of Oslo*, Department. of Geophysics, University of Oslo, 1993.

Komhyr W.D., S.A. Oltmans, J.A. Lathrop, J.B. Kerr, and W.A. Matthews. The latitudinal distribution of ozone to 35 km altitude from ECC ozonesondes observations from 1982-1990. In *Proceedings of Quadrennial ozone symposium* in Charlottesville, Virginia. NASA ref.. publications 3266, pp 858-862, 1994.

Lacis A.A., D.J. Wuebbles and J.A. Logan. Radiative forcing of climate by changes in the vertical distribution of ozone. *J. Geoph. Res*., **95**, 9971-9981, 1990.

Lary D.J., R. Toumi, A.M. Lee, M. Newchurch, M. Pirre and J.B. Renard. Carbon aerosols and atmospheric photochemistry. *J. Geoph. Res*., in press, 1997.

Lelieveld J. and R. van Dorland. Ozone chemistry changes in the troposphere and consequent radiative forcing of climate. In *Atmospheric ozone as a climate gas*. (ed.W.-C. Wang and Isaksen I.S.A.). NATO ASI Series I, **32**, 227-258, Springer Verlag, 1995.

Li, D. and K.P.Shine, A 4-dimensional ozone climatology for UGAMP models. UGAMP Internal Report No 35. Available from Centre for Global Atmospheric Modelling, Dept of Meteorology, Univ of Reading, Reading RG6 6BB, UK, 1995.

Liang, X,-Z, and W.-C. Wang. A GCM study of the climatic effect of 1979-1992 ozone trend, In: *Atmospheric ozone as a climate gas*, W.-C. Wang and I.S.A. Isaksen (eds), NATO ASI series, Springer, 1995

Lin X., M. Trainer and S.C. Liu. On the non-linearity of the tropospheric ozone production. *J. Geoph. Res*., **93**, 15,879-15,888, 1988.

Logan J.A. Tropospheric ozone : Seasonal behaviour, Trends and anthropogenic influence. *J. Geoph. Res.,* **90**, 10463-10482, 1985.

Logan J.A. Trends in vertical distribution of ozone variations from ozonesonde data. *J. Geoph. Res*., **99**, 25553-25585, 1994.

Marenco A., H. Gouget, P. Nedelec, J-P Pages and F.Karcher. Evidence of long term increase in tropospheric ozone from Pic de Midi data series - consequences: positive radiative forcing. *J. Geoph. Res.*, **99**, 16617-16632, 1994.

Müller J.F. and G. Brasseur. IMAGES: A three-dimensional chemical transport model of the global troposphere. *J. Geoph. Res.*, **100**, 16445-16490, 1995.

Myhre G., and F. Stordal. The role of spatial and temporal averaging and clouds in the computation of radiative forcing and GWP, Accepted for publication in *J. Geoph. Res*, 1997

Myhre G., F. Stordal, B. Rognerud and I.S.A. Isaksen. Radiative forcing due to stratospheric ozone. Paper presented at the 'Quadrennial Ozone Symposium' in l'Aquila, September, 1996.

Novelli P.C., P. Steele and P. Tans. Mixing ratios of carbon monoxide in the troposphere. *J. Geoph. Res.,* **97**, 20731-20750, 1992.

Oltmans S.J. and H. Levy II. Surface ozone measurements from a global network. *Atm. Envir.,* **28**, 9-24, 1994.

Prather M. Numerical advection by conservation of second-order moments. *J. Geoph. Res.,* **91**, 6671-6681, 1986.

Prather M., M. McElroy, S. Wofsy, G. Russel and D. Rind. Chemistry of the global troposphere: fluorocarbons as tracers of air motion. *J. Geoph. Res*, **92**, 6579-6613, 1987.

Price C., J.Penner and M.Prather. NOx from lightning 1. Global distribution based on cloud physics. *J. Geoph. Res*, **102**, 5929-5941, 1997a.

Price C., J.Penner and M.Prather. NOx from lightning 2. Constraints from the global atmospheric electric circuit. *J. Geoph. Res*, **102**, 5943-5951, 1997b.

Ramanathan, V. and R.E.Dickinson. The role of stratospheric ozone in the zonal and seasonal radiative energy balance of the earth-troposphere system. *J.Atmos.Sci.,* **36,** 1084-1104, 1979.

Ramaswamy,V. and M.M.Bowen. Effects of changes in radiatively active species upon the lower stratospheric temperatures. *J.Geophys.Res.,* **99,** 18909-18921, 1994.

Ramaswamy V., M.D. Schwarzkopf and W.J. Randel. Fingerprint of ozone depletion in the spatial and temporal pattern of recent stratospheric cooling. *Nature,* **382,** 616-618, 1996

Reichardt J., A. Ansmann, M Serwazi, C. Veitkamp and W. Michaelis. Unexpectedly low ozone concentration in midlatitude tropospheric ice clouds. *Geophys.Res.Lett.,* **23,** 1929-1932, 1996.

Roelofs G.-J. and J. Lelieveld. Model study of the influence of the cross tropopause ozone transport on the ozone levels. *Tellus,* **49B,** 38-55, 1997

Rossow, W.B., and R.A. Schiffer. ISCCP cloud data products, *Bull. Amer. Meteor. Soc.*, **72**, 2-20, 1991

Rothman, L.S., R.R.Gamache, R.H.Tipping, C.P.Rinsland, M.A.H.Smith, D.C.Benner, V.M.Devi, J-M.Flaud, C.Camy-Peyret, A.Perrin, A.Goldman, S.T.Massie, L.R.Brown and

R.A.Toth. The HITRAN molecular database: Editions of 1991 and 1992. *J.Quant.Spectrosc.Radiat.Transf.,* **48,** 469-507, 1992

Santer, B. D., K. E. Taylor, T. M. L. Wigley, T. C. Johns, P. D. Jones, D. J. Karoly, J. F. B. Mitchell, A. H. Oort, J. E. Penner, V. Ramaswamy, M. D. Schwarzkopf, R. J. Stouffer and S. Tett, A search for human influences on the thermal structure of the atmosphere. *Nature*, **382,** 39-46, 1996.

Shine, K.P. On the relative greenhouse strength of gases such as the halocarbons. *J.Atmos.Sci.,* **48,** 1513-1518, 1991

Shine, K.P., B.P.Briegleb, A.S.Grossman, D.Hauglustaine, H.Mao, V.Ramaswamy, M.D.Schwarzkopf, R.van Dorland and W-C.Wang. Radiative forcing due to changes in ozone: a comparison of different codes. In "*Atmospheric ozone as a climate gas*", W-C.Wang and I.S.A.Isaksen (eds), NATO ASI series, Springer, 373-396. 1995.

Staehelin J. and W. Schmid. Trend analysis of tropospheric ozone concentrations utilizing the 20 years data set of ozone balloon and soundings over Payerne (Switzerland). *Atm. Envir.,* **25A**, 1739-1749, 1991.

Stamnes, K., S.-C. Tsay, W. Wiscombe, and K. Jayaweera. A numerically stable algorithm for discrete-ordinate-method radiative transfer in multiple scattering and emitting layered media, *Applied Optics*, **27**, 2502-2509, 1988

Stordal, F. A wide band model for transfer of infrared radiation: Altitude, latitudinal and yearly variation of cooling rates in the troposphere and the stratosphere, *Rep. no. 68, Department of Geophysics*, University of Oslo, 1988.

Stordal, F., T.A. Larsen, G. Myhre, L. Zetterberg. Radiative impacts of ozone and other radiatively active components, *Norwegian Institute for Air Research, OR 26/96*, 1996.

Volz A. and D. Kley. Evaluation of the Montsouris series of ozone measurements made in the nineteenth century. *Nature*, **332**, 240-242, 1988.

Wang W.-C. and N.D. Sze Coupled effects of atmospheric N_2O and O_3 on the Earth's climate. *Nature*, **286**, 589-590, 1980.

Wang, W-C., Y.C.Zhuang and R.D.Bojkov, Climate implications of observed changes in ozone vertical distributions at middle and high latitudes of the northern hemisphere. *Geophys.Res.Lett.,* **20,**1567-1570, 1993.

Wang W.-C., X.-Z. Liang, M.P. Dudek, D.Pollard and S.L. Thompson. Atmospheric ozone as a climate gas. *Atmospheric Research*, **37**, 247-256, 1995.

Wang, W.-C., H. Mao, I. S. A. Isaksen, J. S. Fuglestvedt, and S. Karlsdottir. Indirect effects of increasing atmospheric methane on the radiative forcing through climate-chemistry interactions. To appear in proceedings from XVIII Quadrennial Ozone Symposium, L'Aquila, September, 1996.

WMO, 1994. Scientific assessment of ozone depletion. World Meteorological Organization, Global ozone research and monitoring project. Report No 37, 1994.

Figure Captions

Figure 12. Calculated change in annual mean tropospheric column ozone in dobson units (DU) between the 1850 and the1990 cases.

Figure 15. Radiative forcing (in Wm^{-2}) calculated using the Reading model due to the change in tropospheric ozone since pre-industrial times from the Chemical Transport Model. The annual-mean cloudy-sky adjusted forcing is shown. (a) Thermal infrared, (b) Shortwave and (c) Net.

Figure 16. As Figure 15, but for the OsloRad model.

Figure 17. Radiative forcing (in Wm^{-2}) calculated using the Reading model due to a change in ozone mixing ratio of 10 ppbv everywhere in the troposphere. The annual-mean cloudy-sky forcing is shown. (a) thermal infrared, (b) Shortwave and (c) Net. The contour interval is ...

Figure 18. Yearly variation of the global mean (Gl), northern hemispheric (NH), and southern hemispheric (SH) cloudy-sky adjusted radiative forcing (in Wm^{-2}) calculated using the OsloRad model due to the change in tropospheric ozone since pre-industrial times from the Chemical Transport Model. (a) Thermal infrared, (b) Shortwave and (c) Net. Note that the shortwave calculations are without clouds.

Figure 19. Stratospheric temperature changes (in K) as a function of latitude and altitude calculated using the fixed dynamical heating approximation and the tropospheric ozone changes from the CTM. The values are for July and are from the Reading model. The contour interval is 0.02 K for magnitudes below 0.1 K and then contours are at -0.1, -0.2, -0.4 and -0.6 K.

This is CICERO

CICERO was established by the Norwegian government in April 1990 as a non-profit organization associated with the University of Oslo.

The research concentrates on:

- International negotiations on climate agreements. The themes of the negotiations are distribution of costs and benefits, information and institutions.

- Global climate and regional environment effects in developing and industrialized countries. Integrated assessments include sustainable energy use and production, and optimal environmental and resource management.

- Indirect effects of emissions and feedback mechanisms in the climate system as a result of chemical processes in the atmosphere.

Contact details:

CICERO
P.O. Box. 1129 Blindern
N-0317 OSLO
NORWAY

Telephone: +47 22 85 87 50
Fax: +47 22 85 87 51
Web: www.cicero.uio.no
E-mail: admin@cicero.uio.no